Received: 26 February 2021 | Accepted: 8 June 2021

DOI: 10.1111/bpa.13001

Brain Pathology

RESEARCH ARTICLE

Role of VAPB and vesicular profiles in α-synuclein aggregates in multiple system atrophy

Fumiaki Mori[1] | **Yasuo Miki**[1] | **Kunikazu Tanji**[1] | **Tomoya Kon**[2] | **Masahiko Tomiyama**[2] | **Akiyoshi Kakita**[3] | **Koichi Wakabayashi**[1]

[1]Department of Neuropathology, Hirosaki University Graduate School of Medicine, Hirosaki, Japan

[2]Department of Neurology, Hirosaki University Graduate School of Medicine, Hirosaki, Japan

[3]Department of Pathology, Brain Research Institute, Niigata University, Niigata, Japan

Correspondence
Fumiaki Mori, Department of Neuropathology, Institute of Brain Science, Hirosaki University Graduate School of Medicine, 5 Zaifu-cho, Hirosaki 036-8562, Japan. Email: neuropal@hirosaki-u.ac.jp

Funding information
Japan Society for the Promotion of Science, Grant/Award Number: 17K07088, 18H02533, 20K06887 and 21K07452; Hirosaki University Institutional Research Grant

Abstract

The pathological hallmark of multiple system atrophy (MSA) is fibrillary aggregates of α-synuclein (α-Syn) in the cytoplasm and nucleus of both oligodendrocytes and neurons. In neurons, α-Syn localizes to the cytosolic and membrane compartments, including the synaptic vesicles, mitochondria, and endoplasmic reticulum (ER). α-Syn binds to vesicle-associated membrane protein-binding protein B (VAPB) in the ER membrane. Overexpression of wild-type and familial Parkinson's disease mutant α-Syn perturbs the association between the ER and mitochondria, leading to ER stress and ultimately neurodegeneration. We examined brains from MSA patients (n = 7) and control subjects (n = 5) using immunohistochemistry and immunoelectron microscopy with antibodies against VAPB and phosphorylated α-Syn. In controls, the cytoplasm of neurons and glial cells was positive for VAPB, whereas in MSA lesions VAPB immunoreactivity was decreased. The proportion of VAPB-negative neurons in the pontine nucleus was significantly higher in MSA (13.6%) than in controls (0.6%). The incidence of cytoplasmic inclusions in VAPB-negative neurons was significantly higher (42.2%) than that in VAPB-positive neurons (3.6%); 67.2% of inclusion-bearing oligodendrocytes and 51.1% of inclusion-containing neurons were negative for VAPB. Immunoelectron microscopy revealed that α-Syn and VAPB were localized to granulofilamentous structures in the cytoplasm of oligodendrocytes and neurons. Many vesicular structures labeled with anti-α-Syn were also observed within the granulofilamentous structures in the cytoplasm and nucleus of both oligodendrocytes and neurons. These findings suggest that, in MSA, reduction of VAPB is involved in the disease process and that vesicular structures are associated with inclusion formation.

KEYWORDS
electron microscopy, glial cytoplasmic inclusion, multiple system atrophy, vesicle-associated membrane protein-binding protein B, α-synuclein

1 | INTRODUCTION

Multiple system atrophy (MSA) is a fatal neurodegenerative disease characterized by a combination of various degrees of parkinsonism, cerebellar ataxia, and autonomic failure. MSA is now divided into two clinical subtypes: MSA with predominant parkinsonian features (MSA-P) and MSA with predominant cerebellar dysfunction (MSA-C). The pathological hallmark of MSA is widespread glial cytoplasmic inclusions (GCIs) in oligodendrocytes, which contain fibrillary aggregates of α-synuclein (α-Syn) (1). Neuronal cytoplasmic inclusions (NCIs) consisting of fibrillary aggregates of α-Syn are also found in certain areas of the brain, including the neostriatum, substantia nigra, pontine nucleus, and inferior olivary nucleus (2). Moreover, α-Syn aggregates are also seen in the nucleus of oligodendrocytes and neurons, being referred to as glial nuclear inclusions (GNIs) and neuronal nuclear inclusions (NNIs), respectively (3, 4). In Parkinson's disease (PD) and dementia with Lewy bodies (DLB), fibrillary aggregates of α-Syn occur in the cytoplasm of neurons and glial cells (astrocytes and oligodendrocytes) (5). Therefore, MSA, PD, and DLB are collectively referred to as α-synucleinopathies. However, in PD and DLB, α-Syn aggregates are not noted in the nucleus. Thus, the formation of GNIs and NNIs distinguishes MSA from PD and DLB.

Under normal conditions, α-Syn is enriched in the presynapses and perinuclear region of neurons. In neurons, α-Syn localizes to the cytosolic and membrane compartments, including the synaptic vesicles, mitochondria, and endoplasmic reticulum (ER) (6–9). Vesicle-associated membrane protein-binding protein B (VAPB) exists in the ER membranes and binds to protein tyrosine phosphatase interacting protein 51 (PTPIP51) in the mitochondrial outer membranes, in order to tether the ER to mitochondria (10). Paillusson et al. have reported that α-Syn binds to VAPB in the ER membrane and that overexpression of wild-type and familial PD mutant α-Syn disrupts the tethering between VAPB in the ER and PTPIP51 in the mitochondria and weakens the association between the ER and mitochondria, leading to ER stress, and ultimately neurodegeneration (11). This disruption is seen in neurons derived from induced pluripotent stem cells from familial PD patients harboring pathogenic triplication of the α-Syn gene (11). These findings prompted us to examine the alteration of VAPB in patients with MSA. In the present study, we demonstrated for the first time that VAPB immunoreactivity is significantly decreased in MSA lesions. We further examined brain specimens from MSA patients using immunoelectron microscopy. Ultrastructural examination revealed that fibrillary aggregates of α-Syn in the oligodendroglial and neuronal inclusions (GCIs, GNIs, NCIs, and NNIs) contain many vesicular structures. We discuss the significance of VAPB and vesicular structures in the formation of α-Syn inclusions in MSA.

2 | MATERIALS AND METHODS

2.1 | Subjects

Twelve autopsy cases were included in this study (Table 1). Seven patients with MSA (age 49–89 years, average = 68.0 years) were confirmed at autopsy by the presence of numerous GCIs. All of the MSA cases lacked Lewy body pathology. The clinical and neuropathological features of a case of minimal change (early stage) MSA (case 1) have been reported previously (12).

TABLE 1 List of subjects

No.	Group	Age at death (years)	Gender	Disease duration (years)	Clinical/pathological diagnosis	No. of neurons per 0.25 mm^2
1	MSA	57	F	1	MSA-C	225
2	MSA	71	M	1	MSA-P	241
3	MSA	89	M	4	MSA-P	359
4	MSA	61	M	4.5	MSA-P	64
5	MSA	83	F	5	MSA-P	375
6	MSA	49	F	7	MSA-P	86
7	MSA	66	M	13	MSA-C	225
	Average	68.0				225.0
8	Cont	53	M		Normal brain	353
9	Cont	60	M		Normal brain	473
10	Cont	67	F		Normal brain	433
11	Cont	71	F		Arteriosclerosis in the brain	453
12	Cont	84	M		Normal brain	468
	Average	67.0				436.0

Abbreviations: NA, not available; NCI, neuronal cytoplasmic inclusion; NNI, neuronal nuclear inclusion; VAPB, vesicle-associated membrane protein (VAMP)-binding protein B.

Five patients were used as controls (age 53–84 years, average = 67.0 years).

2.2 | Immunohistochemistry

Four-micrometer-thick sections of the basal ganglia, midbrain, pons, medulla oblongata, and cerebellum were cut and subjected to immunohistochemical processing using the avidin-biotin-peroxidase complex (ABC) method with a Vectastain ABC kit (Vector, Burlingame, CA, USA). Antibodies against phosphorylated α-Syn (p-α-Syn) (#64; Wako, Osaka, Japan; 1:5000) and VAPB (HPA013144; Sigma, St. Louis, MO, USA; 1:250) were used as primary antibodies. The sections were pretreated in an autoclave for 10 min in 10 mM citrate buffer (pH 6.0) for antigen retrieval. For p-α-Syn immunohistochemistry, the sections were additionally pretreated in 98% formic acid for 5 min. Diaminobenzidine was used as the chromogen. The sections were counterstained with hematoxylin.

2.3 | Cell counts of VAPB-positive and -negative neurons

In each case of MSA and in the controls, the numbers of VAPB-positive and -negative neurons in the pontine nucleus were counted on one section immunostained with anti-VAPB. Counting was performed in 10 fields of the pontine nucleus at ×200 original magnification using an eyepiece graticule with parallel sweeps of the microscope stage. The average number was considered to be the value for each case.

In each case of MSA, sections were double immunolabeled with combinations of polyclonal anti-VAPB (1:250) and monoclonal anti-p-α-Syn (1:5000). Initially, the immunoproduct of anti-VAPB was detected by the ABC method with diaminobenzidine as the chromogen and the sections were counterstained with hematoxylin. Digital images of the sections were captured using a virtual slide system (VS110-S1; Olympus, Tokyo, Japan). After removing the cover glasses from the slides in xylene, the specimens were decolorized, subjected to heat retrieval using an autoclave for 10 min in 10 mM citrate buffer (pH 6.0), and immersed in 95% formic acid for 5 min. The sections were then immunostained with anti-p-α-Syn (1:5000) using the ABC method with alkaline phosphatase as the tertiary reagent and Vector Blue as the chromogen for alkaline phosphatase (Vector). Digital images of the sections were again captured on the virtual slide system. The presence or absence of p-α-Syn-immunoreactive NCIs and NNIs was observed under an ×20 objective lens, confirmed by the virtual slide system, and recorded in each neuron. Finally, the numbers of VAPB-positive and -negative neurons with or without inclusions (NCIs or NNIs) were calculated. Moreover, the average proportion of VAPB-positive inclusions relative to the total number of p-α-Syn-positive inclusions (GCIs or NCIs) was calculated.

2.4 | Immunoelectron microscopy

Fifty-micrometer-thick vibratome sections of the pontine base from three MSA patients (cases 1, 2, and 6) and the cervical spinal cord from a MSA patient (case 1) were incubated with mouse monoclonal anti-p-α-Syn (1:500) or rabbit polyclonal anti-VAPB (1:100) for two days at 4℃, followed by incubation with a 1.4-nm gold-coupled Fab' fragment of goat anti-mouse or anti-rabbit IgG

% of VAPB-negative neurons	NCI incidence in VAPB-positive neurons (%)	NCI incidence in VAPB-negative neurons (%)	NNI incidence in VAPB-positive neurons (%)	NNI incidence in VAPB-negative neurons (%)
7.6	2.6	39.3	13.9	12.5
19.5	7.7	31.6	13.4	4.7
0.8	0	66.7	NA	NA
32.8	5.7	47.8	17.9	20.5
10.1	0	6.7	NA	NA
15.1	4.2	28.6	17.8	18.8
20.4	4.7	75.0	10.1	14.3
15.2	3.6	42.2	14.6	14.2
0	0	0	0	0
0.4	0	0	0	0
0	0	0	0	0
0	0	0	0	0
2.4	0	0	0	0
0.6	0.0	0.0	0.0	0.0

(Nanoprobes, Yaphank, NY, USA). Sections from a control subject (case 10) were also incubated with anti-VAPB. Sections were visualized using a silver enhancing kit (BB International, Cardiff, UK). The immunolabeled sections were post-fixed in 1% osmium tetroxide, stained with uranyl acetate, dehydrated in ethanol, embedded in epoxy resin, and then sectioned and viewed with a JEOL1230 electron microscope (JEOL Ltd., Tokyo, Japan).

To establish the relative abundance of p-α-Syn immunoreactivity in vesicular structures in GCIs (n = 5), GNIs (n = 1), NCIs (n = 5), and NNIs (n = 5), randomly selected areas of each inclusion were photographed from the selected ultrathin sections and used with final magnification 60,000× (13). Quantification of immunogold labeling was carried out in the pontine nucleus totaling approximately 15–35 μm^2. We counted the numbers of immunoparticles identified in vesicles and granulofilamentous structures in each inclusion. The data were expressed as a percentage of the number of immunoparticles in vesicles and granulofilamentous structures relative to the total number of immunoparticles.

2.5 | Statistical analysis

To compare the proportions of VAPB-negative neurons between controls and MSA, the incidences of NCIs in VAPB-positive and -negative neurons, and the proportions of p-α-Syn-positive immunoparticles in the GCIs, NCIs, and NNIs between vesicular and granulofilamentous structures, Student's or Welch's *t*-test was applied. Calculations were performed using Statcel software (OMS Publishing, Tokorozawa, Japan). Differences were considered significant at probability values of less than 0.05 ($p < 0.05$).

3 | RESULTS

3.1 | VAPB immunoreactivity in controls and MSA

In controls, the cytoplasm of neurons in the neostriatum (Figure 1A), substantia nigra (Figure 1C), pontine nucleus (Figure 1E), inferior olivary nucleus (Figure 1G), and cerebellum (Figure 1I) was strongly immunolabeled with anti-VAPB antibody. The cytoplasm of oligodendrocytes and astrocytes was also immunopositive for VAPB (Figure 1K,L). The nuclei of neurons and glial cells were not stained with anti-VAPB. In MSA, VAPB

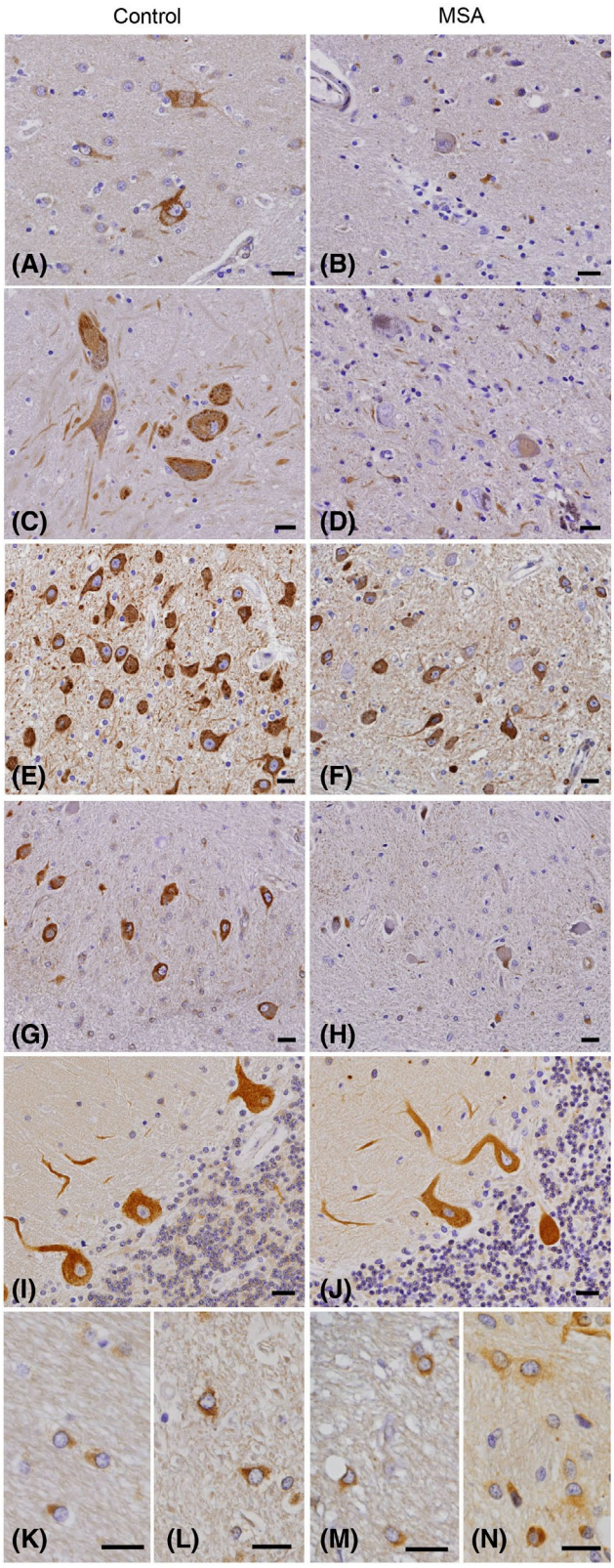

FIGURE 1 Immunoreactivity of vesicle-associated membrane protein-binding protein B (VAPB) in the putamen (A, B), substantia nigra (C, D), pontine nucleus (E, F), inferior olivary nucleus (G, H), cerebellum (I, J) and pontine base (K-N) in controls (A, C, E, G, I, K, L) and multiple system atrophy (MSA) (B, D, F, H, J, M, N). In controls, the cytoplasm of almost all neurons is immunostained (A, C, E, G, I). In MSA, VAPB immunoreactivity is decreased in the putamen (B), substantia nigra (D), pontine nucleus (F), and inferior olivary nucleus (H), but not in Purkinje cells (J). The cytoplasm of oligodendrocytes (K, M) and astrocytes (L, N) is also positive for VAPB in controls (K, L) and MSA (M, N). Bars = 20 μm

immunoreactivity of the neuronal cytoplasm was decreased in the neostriatum (Figure 1B), substantia nigra (Figure 1D), pontine nucleus (Figure 1F), and inferior olivary nucleus (Figure 1H), but not in cerebellar Purkinje cells (Figure 1J). VAPB immunoreactivity of the glial cytoplasm without inclusions was preserved (Figure 1M,N). Although some NCIs and GCIs were also positive for VAPB, the immunoreactivity was usually decreased in these inclusions (Figure 2A,B). No VAPB immunoreactivity was seen in NNIs or GNIs.

The proportion of VAPB-negative neurons relative to the total number of neurons in the pontine nucleus was significantly higher in MSA (13.6%) than in the controls (0.6%) ($p < 0.05$) (Figure 2C).

3.2 | Relationship between VAPB immunoreactivity and inclusion formation

The pontine neurons with NCIs usually showed less intense VAPB immunoreactivity than those without (Figure 2D–G). Double immunolabeling revealed that the incidence of cytoplasmic inclusions in VAPB-negative neurons was significantly higher (42.2%) than that in VAPB-positive neurons (3.6%) ($p < 0.05$) (Figure 2H). There was no significant difference in the incidence of nuclear inclusions between VAPB-negative neurons (14.2%) and VAPB-positive neurons (14.6%). In addition, 67.2% of inclusion-bearing oligodendrocytes and 51.1% of NCI-containing neurons were negative for VAPB.

3.3 | Immunoelectron microscopy

In controls, VAPB immunoreactivity was localized to the rough ER (Figure 3A,B). Similar findings were also seen in neurons without inclusions in MSA.

In the pontine nucleus of patients with MSA, GCIs consisted of granulofilamentous structures (Figure 3C). Vesicular structures were found within the granulofilamentous structures (Figure 3D). Immunoparticles-labeling of VAPB was localized to the granulofilamentous structures, but not to the vesicular structures, of GCIs (Figure 3D). NCIs were also composed of randomly arranged filaments (Figure 3E) and vesicular structures (Figure 3F). Immunoparticles-labeling of VAPB was localized to the granulofilamentous structures, but not to the vesicular structures, of NCIs (Figure 3F). In a case of MSA (case 2), immunolabeling with anti-VAPB was detected in vesicular structures in the pontine nucleus in all of 11 GCIs and 11 NCIs examined.

Immunoparticles-labeling of p-α-Syn was localized to the granulofilamentous and vesicular structures of GCIs and GNIs (Figure 4A–D). In addition to vesicles, tubular structures were observed (Figure 4D). Small vesicles were also observed on and under the nuclear membrane (Figure 4E–G), suggesting entry of p-α-Syn-containing vesicles into the nucleus from the cytoplasm. In the case of early stage MSA (case 1), GCIs contained many vesicles of various sizes (40–180 nm in diameter), and tubulovesicular and tubular structures (Figure 4H,I). In the pontine nucleus immunolabeled with anti-p-α-Syn from three cases of MSA (cases 1, 2, and 6), 14 GCIs and one GNI were examined and p-α-Syn-positive vesicular structures were detected in almost all inclusions.

NCIs contained granulofilamentous and vesicular structures labeled with anti-p-α-Syn (Figure 5A,B). NCIs also contained swollen mitochondria, lysosomes, and lipofuscin granules (Figure 5C). NNIs were composed of granulofilamentous structures, which were often located near the nuclear membrane (Figure 5A,B). NNIs contained many vesicles labeled with immunoparticles (Figure 5D). In the case of early stage MSA (case 1), linear NNIs often appeared as fibrils arranged in bundles (Figure 5E). The fibrils were closely associated with vesicles and tubulovesicular structures (Figure 5F). In the pontine nucleus immunolabeled with anti-p-α-Syn from three cases of MSA (cases 1, 2, and 6), 14 NCIs and 13 NNIs were examined and p-α-Syn-positive vesicular structures were detected in almost all inclusions.

Quantitative analysis revealed the proportions of p-α-Syn-positive immunoparticles in vesicular versus granulofilamentous structures in GCIs (57.6% vs. 42.4%), GNIs (80.0% vs. 20.0%), NCIs (67.8% vs. 32.2%) and NNIs (71.9% vs. 28.1%). The proportions of p-α-Syn-positive immunoparticles in the vesicular structures were significantly higher than those in the granulofilamentous structures in GCIs, NCIs, and NNIs ($p < 0.01$).

4 | DISCUSSION

In the present study, we demonstrated for the first time that VAPB immunoreactivity was significantly decreased in MSA lesions, especially in oligodendrocytes and neurons with α-Syn aggregates. Moreover, immunoelectron microscopy revealed that vesicular structures immunoreactive for p-α-Syn were closely associated with fibrillary aggregates in the cytoplasm and nucleus of both oligodendrocytes and neurons (GCIs, GNIs, NCIs, and NNIs).

Under normal conditions, VAPB functions as a tethering molecule at the sites of membrane contact between the ER and intracellular organelles. VAPB regulates a wide variety of cellular functions, including lipid transport, membrane trafficking, microtubule reorganization, and unfolded protein response (14). In the present study, the proportion of VAPB-negative neurons relative to the total number of neurons in the pontine nucleus was significantly higher in MSA (13.6%) than in the controls (0.6%). VAPB immunoreactivity of the neuronal cytoplasm was also decreased in the neostriatum, substantia nigra, and inferior olivary nucleus, but

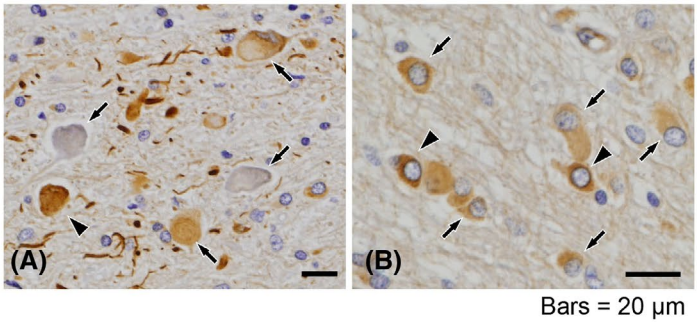

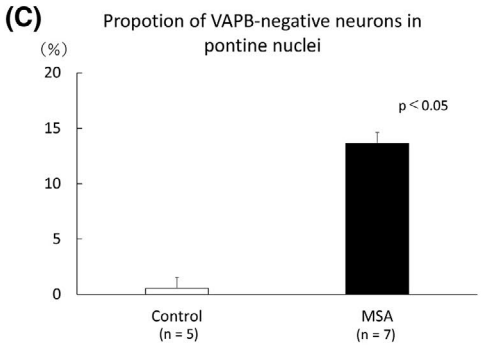

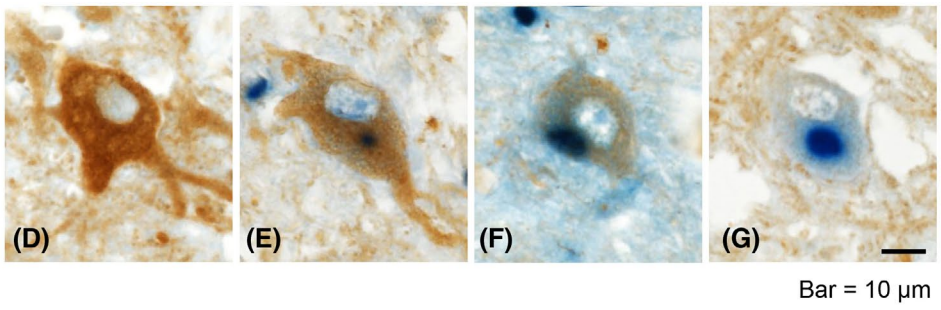

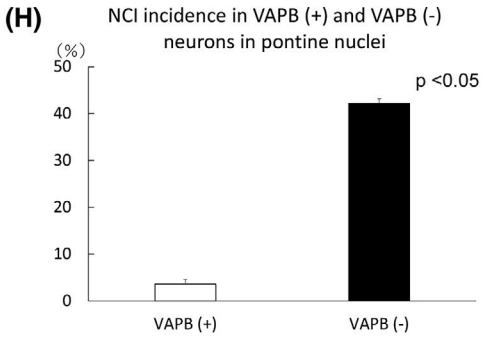

FIGURE 2 VAPB immunoreactivity in neuronal and glial inclusions in the pontine nucleus in MSA (A, B). (A) Neuronal cytoplasmic inclusions (NCIs) showing no or weak immunoreactivity for VAPB (arrows). Note that swollen neurites and a small proportion of NCIs (arrowheads) show intense immunoreactivity. (B) Oligodendrocytes with cytoplasmic inclusions showing less intense VAPB immunoreactivity (arrows) than those without (arrowheads). Bars = 20 μm. (C) The proportion of VAPB-negative neurons relative to the total number of neurons in the pontine nucleus. The proportion is significantly higher in MSA (13.6%) than in controls (0.6%) ($p < 0.05$). (D–G) Double immunostaining for VAPB (brown) and phosphorylated α-synuclein (p-α-Syn) (blue) in the pontine neurons in the case of MSA (case 6). (D) A pontine neuron without p-α-Syn aggregates showing strong cytoplasmic immunoreactivity for VAPB. (E) A pontine neuron with focal cytoplasmic staining for p-α-Syn showing moderate cytoplasmic immunoreactivity. (F) Another pontine neuron with a small p-α-Syn aggregate showing weak cytoplasmic immunoreactivity. (G) Another pontine neuron with a typical NCI showing no cytoplasmic immunoreactivity. Bar = 10 μm. (H) The incidence of NCIs in the pontine nucleus in MSA. The incidence of NCIs in VAPB-negative neurons is significantly higher (42.2%) than that in VAPB-positive neurons (3.6%) ($p < 0.05$)

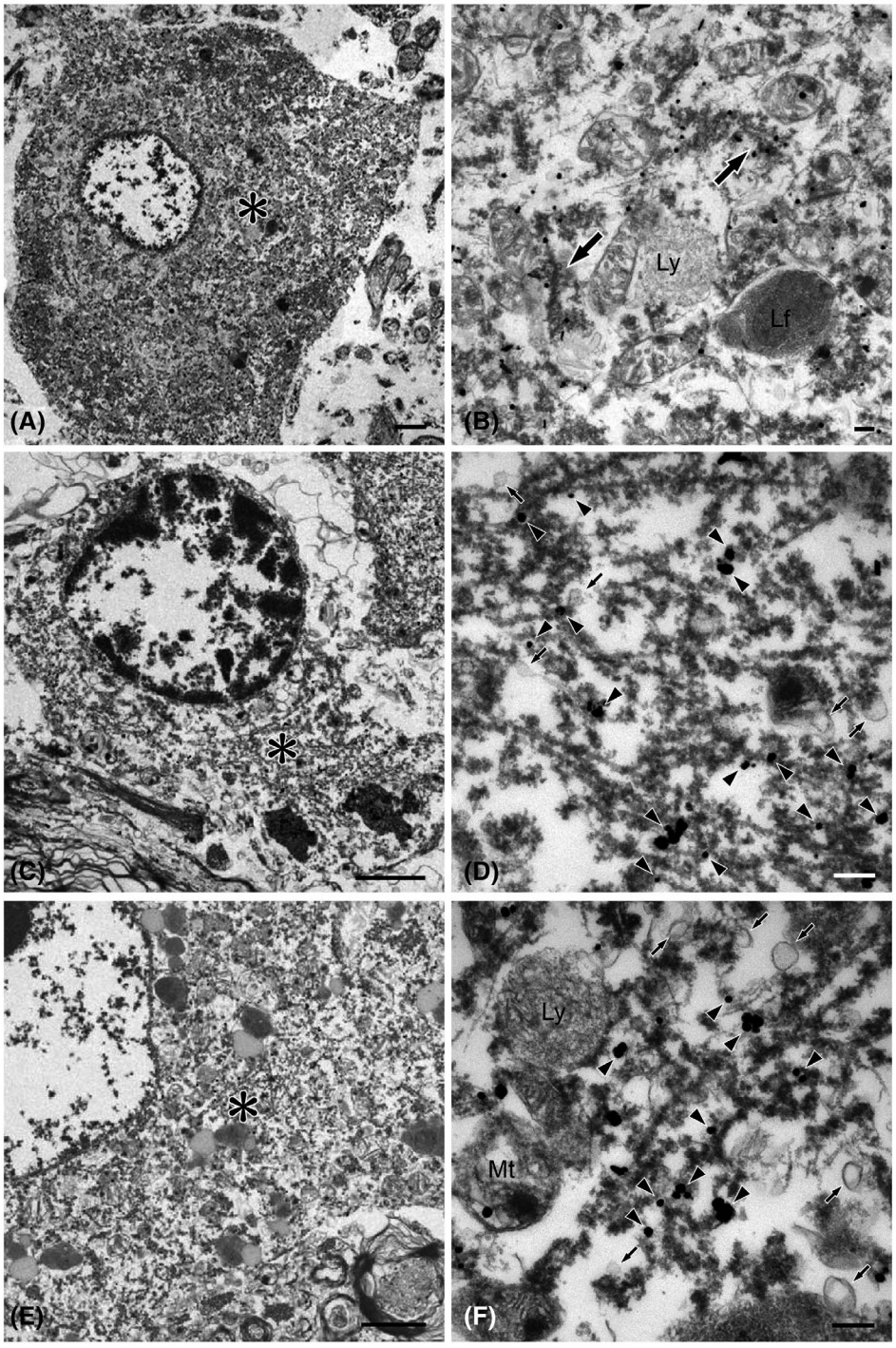

FIGURE 3 Immunoelectron microscopy of normal neurons in the pontine nucleus labeled with anti-VAPB in a control subject (case 10) (A, B). (B) A higher-magnification view of the area indicated by the asterisk in (A) showing rough endoplasmic reticulum labeled with immunoparticles (arrows). Ly, lysosomes; Lf, lipofuscin granules. Immunoelectron microscopy of glial cytoplasmic inclusions (GCIs) in the pontine nucleus labeled with anti-VAPB in a case of MSA (case 2) (C, D). (C) An oligodendrocyte containing a GCI (asterisk). (D) A higher-magnification view of the area indicated by the asterisk in (C) showing granulofilamentous structures, vesicles, and mitochondria (Mt). Note that VAPB is localized to the filaments (arrowheads), but not to the vesicular structures (arrows). Immunoelectron microscopy of NCIs in the pontine nucleus labeled with anti-VAPB in a case of MSA (case 2) (E, F). (E) A neuron containing a tiny NCI (asterisk). (F) A higher-magnification view of the area indicated by the asterisk in (E) showing mitochondria (Mt), lysosomes (Ly) and granulofilamentous structures labeled with immunoparticles (arrowheads). Note that vesicular structures are not labeled with immunoparticles (arrows). Bars = 2 μm in A, C, E; 0.2 μm in B, D, F

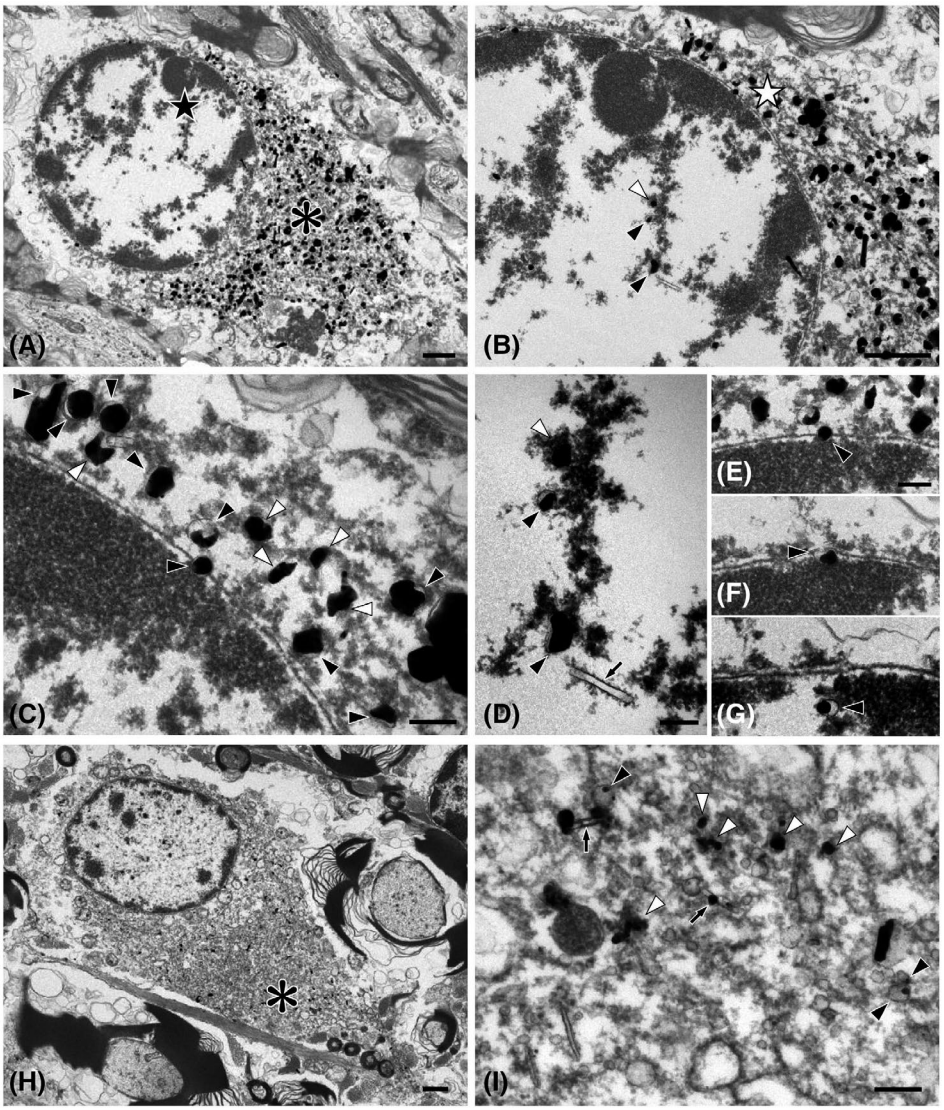

FIGURE 4 Immunoelectron microscopy of GCIs and glial nuclear inclusions (GNIs) in the pontine nucleus labeled with anti-p-α-Syn in a case of MSA (case 2) (A-G). (A) An oligodendrocyte containing a GCI (asterisk) and a GNI (black star). (B) A higher-magnification view of the area indicated by the black star in (A) showing vesicular and granulofilamentous structures labeled with immunoparticles. (C) A higher-magnification view of the area indicated by the white star in (B) showing some vesicles (black arrowheads), and granulofilamentous structures (white arrowheads) labeled with immunoparticles. (D) A higher-magnification view of the area indicated by the black star in (A) showing some vesicles (black arrowheads) and granulofilamentous structures (white arrowheads) labeled with immunoparticles and a tubular structure (arrow). (E-G) Small vesicles labeled with immunoparticles (black arrowheads) are seen on (E), beneath (F) and under the nuclear membrane (G). Immunoelectron microscopy of GCIs in the spinal white matter labeled with anti-p-α-Syn in the case of early stage MSA (case 1) (H, I). (H) An oligodendrocyte containing a GCI (asterisk). (I) A higher-magnification view of the area indicated by the asterisk in (H) showing many vesicles (40–180 nm in diameter), and tubular and tubulovesicular structures. Some vesicles (arrowheads), granulofilamentous structures (white arrowheads) and tubular structures (arrows) are labeled with immunoparticles. Bars = 1 μm in A, B, H; 0.2 μm in C-G, I

not in cerebellar Purkinje cells. This is in line with the finding that α-Syn is accumulated in the neuronal cytoplasm in the neostriatum, substantia nigra, pontine nucleus, and inferior olivary nucleus, but not in cerebellar Purkinje cells, in MSA (2, 15). Moreover, the incidence of NCIs in VAPB-negative neurons was significantly higher (42.2%) than that in VAPB-positive neurons (3.6%); 67.2% of inclusion-bearing oligodendrocytes and 51.1% of inclusion-containing neurons were negative for VAPB. Immunoelectron microscopy revealed that VAPB was localized to the granulofilamentous structures of GCIs and NCIs. These findings suggest that reduction of VAPB is closely associated with aggregation of α-Syn in MSA.

As for the reduction of VAPB, some cellular processes might play a role in degrading VAPB. Tanji et al. reported that NEDD8 ultimate buster 1 (NUB1) suppresses the formation of Lewy body-like inclusions by proteasomal degradation of synphilin-1 (16). Moreover, the latter authors demonstrated immunohistochemical localization of NUB1 in neuronal and glial inclusions (NCIs, NNIs, GCIs, and GNIs) in MSA (17). Recently,

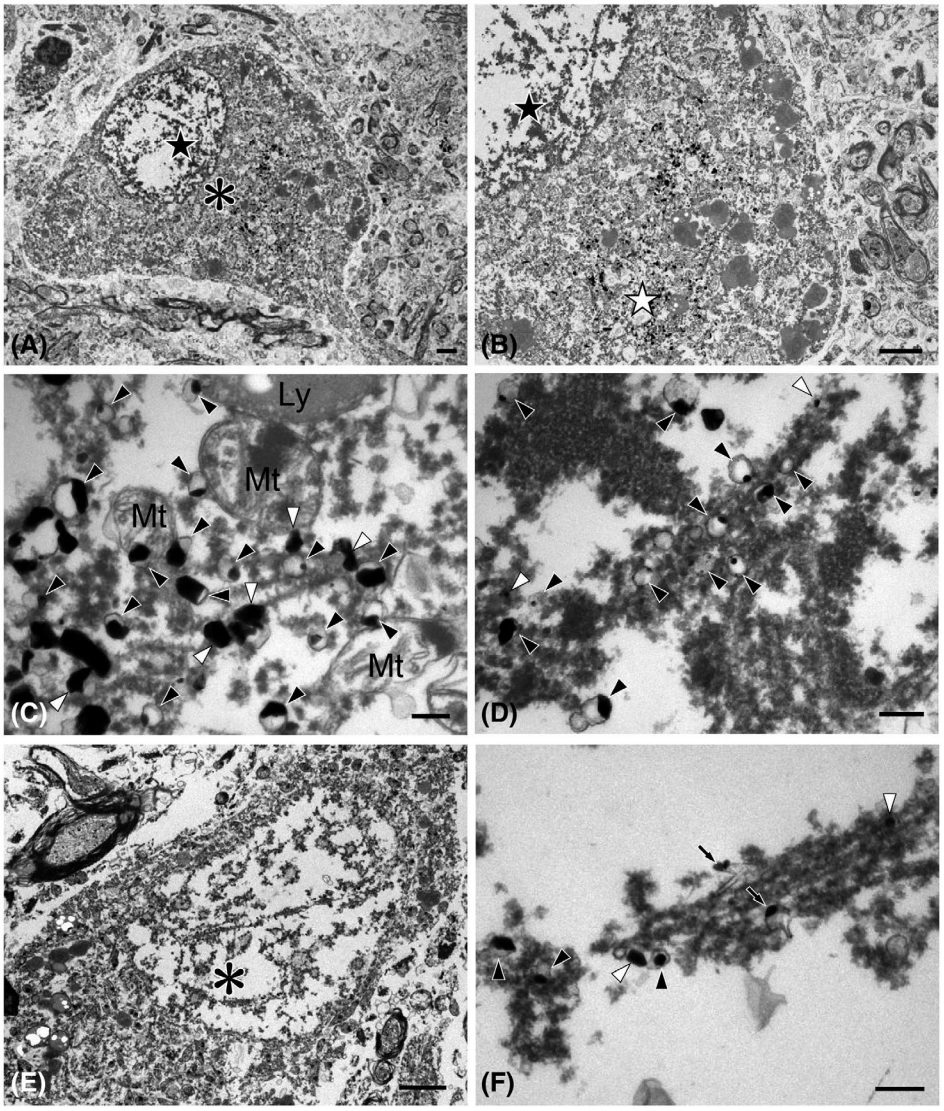

FIGURE 5 Immunoelectron microscopy of NCIs and neuronal nuclear inclusions (NNIs) in the pontine nucleus labeled with anti-p-α-Syn in a case of MSA (case 2) (A-D). (A) A neuron containing an NCI (asterisk) and an NNI (black star). (B) A higher-magnification view of the area indicated by the asterisk in (A) showing an NCI labeled with immunoparticles (white star) near lipofuscin granules. An NNI (black star) is attaching to the nuclear membrane. (C) A higher-magnification view of the area indicated by the white star in (B) showing vesicles (black arrowheads) and granulofilamentous structures (white arrowheads) labeled with immunoparticles in association with swollen mitochondria (Mt) and lysosomes (Ly). (D) A higher-magnification view of the area indicated by the black star in (B) showing vesicles (black arrowheads) and granulofilamentous structures (white arrowheads) labeled with immunoparticles. Immunoelectron microscopy of NNIs in the pontine nucleus labeled with anti-p-α-Syn in the case of early stage MSA (case 1) (E, F). (E) A neuron containing NNIs (asterisk). (F) A higher-magnification view of the area indicated by the asterisk in (E) showing vesicules (black arrowheads), tubulovesicular structures (arrows), and granulofilamentous structures (white arrowheads) labeled with immunoparticles. Bars = 2 μm in A, B, E; 0.2 μm in C, D, F

Li et al. reported that NUB1L protein promotes the proteasomal degradation of misfolded proteins (18). In the present study, VAPB was localized to the granulofilamentous structures of GCIs and NCIs. It is possible to consider that both NUB1 and VAPB suppress the formation of α-Syn aggregates in MSA. However, further studies are needed to prove the relationship between NUB1 and VAPB.

ER-mitochondria signaling is mediated by interactions between the integral ER protein VAPB and the outer mitochondrial membrane protein PTPIP51. These VAPB-PTPIP51 tethers are known to regulate a number of ER-mitochondria signaling functions including delivery of Ca^{2+} from ER stores to mitochondria, mitochondrial ATP production, autophagy, and synaptic activity. α-Syn binds to VAPB in the ER membrane (11). Overexpression of wild-type and familial PD mutant α-Syn disrupts the tethering between VAPB and PTPIP51, which disturbs Ca^{2+} homeostasis and mitochondrial ATP production (11). The temporal cortex of patients with Alzheimer's disease shows a reduced level of VAPB (19). Thus it is possible to consider that the VAPB-PTPIP51 tethers are disrupted in certain neurodegenerative disorders.

α-Syn can bind to lipid membranes to perform physiological functions (20) or form a tetramer with an α-helical structure that can resist abnormal aggregation (21). In familial PD with missense mutations of the α-Syn gene, a tendency for α-Syn to aggregate on lipid membranes has been observed (22). In addition, in PARK14, which is assumed to have membrane lipid abnormalities, fibrillary aggregates of α-Syn (Lewy bodies) have been confirmed by autopsy (23). Recent studies using correlative light and electron microscopy and tomography on postmortem brain tissue from patients with PD have demonstrated that α-Syn-immunopositive Lewy pathology is characterized by membrane crowding, including vesicular structures and dysmorphic organelles (mitochondria and lysosomes) (24). These findings support the idea that aggregation of α-Syn promotes the disruption of membrane homeostasis or trafficking in neurons, leading to the formation of Lewy bodies (25).

The ultrastructure of GCIs was first reported in patients with MSA by Papp et al. in 1989 (26). They reported that GCIs are composed of tubular structures. The ultrastructure of NCIs was first described in the pontine nucleus in MSA by Kato et al. in 1990 (27). They reported that NCIs are composed of granulofilamentous structures. To the best of our knowledge, vesicular structures have not been reported in glial and neuronal inclusions in MSA. It is noteworthy that 'circular profiles' were described within granulofilamentous structures of GCIs, GNIs, and NCIs by Papp and Lantos in 1992 (4). These structures are similar to circular profiles observed in the central core of brainstem-type Lewy bodies in PD (28). However, subsequent ultrastructural studies did not note the circular profiles in MSA inclusions (3, 29–44). Our ultrastructural examination revealed that vesicular structures were consistently present in α-Syn aggregates (GCIs, GNIs, NCIs, and NNIs) in MSA, and α-Syn immunoreactivity was confirmed in these vesicular structures. The present findings suggest that vesicular structures play an important role in the fibrillary aggregation of α-Syn in MSA.

In the present study, vesicular structures containing p-α-Syn were detected near the nuclear membrane (Figure 4E–G), indicating that α-Syn might be transported from the cytoplasm to the nucleus by membrane trafficking. Under normal conditions, α-Syn is localized to the neuronal nucleus throughout the brain (45). It has been reported that mono-ubiquitination (46) and oxidative stress (47, 48) induce nuclear translocation of α-Syn in cultured neuronal cells. Schneider et al. reported that α-Syn was detectable in both the cytoplasm and nucleus of cultured neuronal cells, and when over-expressed, frequently formed clusters around cytoplasmic microvesicles of unknown function (49). Although α-Syn lacks an obvious nuclear localization signal, tagging proteins with such sequences have been widely used to help clarify the behavior of proteins in specific subcellular compartments. However, the lipid bilayer can fuse with other bilayers such as the cell membrane, delivering the liposome contents, although this is a complex and non-spontaneous event (50). It has been reported that α-Syn might be transported within extracellular vesicles in both directions, from the blood to the brain and from the brain to the blood (51, 52). These findings support the hypothesis that transneuronal propagation of misfolded proteins is involved in the progression of neurodegenerative proteinopathies, including MSA (53).

In conclusion, in MSA, reduction of VAPB is involved in the disease process and vesicular structures are associated with the formation of α-Syn inclusions. Blocking the process of α-Syn aggregation at an earlier stage would repress the progression of MSA.

ACKNOWLEDGMENTS

This work was supported by JSPS KAKENHI Grant Numbers 17K07088 (F.M.), 21K07452 (Y.M), 20K06887 (K.T.), and 18H02533 (K.W.) and a Hirosaki University Institutional Research Grant (K.W.). The authors wish to express their gratitude to Ms. M. Nakata for her technical assistance.

CONFLICT OF INTEREST

All authors have no conflicts of interest to disclose.

AUTHOR CONTRIBUTIONS

Fumiaki Mori: study concept and design, drafting the manuscript, and acquisition of data (neuropathological examination). Yasuo Miki, Tomoya Kon, and Masahiko Tomiyama: acquisition of clinical data. Kunikazu Tanji, Akiyoshi Kakita, and Koichi Wakabayashi: study concept and design, acquisition of data (neuropathological examination), and study supervision. All authors read and approved the final manuscript.

DATA AVAILABILITY STATEMENT

The datasets generated during and/or analysed during the current study are available from the corresponding author on reasonable request.

ORCID

Fumiaki Mori https://orcid.org/0000-0003-1903-1766

REFERENCES

1. Wakabayashi K, Yoshimoto M, Tsuji S, Takahashi H. Alpha-synuclein immunoreactivity in glial cytoplasmic inclusions in multiple system atrophy. Neurosci Lett. 1998;249:180–2.
2. Ozawa T, Paviour D, Quinn NP, Josephs KA, Sangha H, Kilford L, et al. The spectrum of pathological involvement of the striatonigral and olivopontocerebellar systems in multiple system atrophy: clinicopathological correlations. Brain. 2004;127:2657–71.
3. Lin WL, DeLucia MW, Dickson DW. Alpha-synuclein immunoreactivity in neuronal nuclear inclusions and neurites in multiple system atrophy. Neurosci Lett. 2004;354:99–102.
4. Papp MI, Lantos PL. Accumulation of tubular structures in oligodendroglial and neuronal cells as the basic alteration in multiple system atrophy. J Neurol Sci. 1992;107:172–82.

5. Wakabayashi K, Hayashi S, Yoshimoto M, Kudo H, Takahashi H. NACP/alpha-synuclein-positive filamentous inclusions in astrocytes and oligodendrocytes of Parkinson's disease brains. Acta Neuropathol. 2000;99:14–20.
6. Guardia-Laguarta C, Area-Gomez E, Rüb C, Liu Y, Magrané J, Becker D, et al. α-Synuclein is localized to mitochondria-associated ER membranes. J Neurosci. 2014;34:249–59.
7. Guardia-Laguarta C, Area-Gomez E, Schon EA, Przedborski S. Novel subcellular localization for α-synuclein: possible functional consequences. Front Neuroanat. 2015;9:17.
8. Guerrero E, Vasudevaraju P, Hegde ML, Britton GB, Rao KS. Recent advances in α-synuclein functions, advanced glycation, and toxicity: implications for Parkinson's disease. Mol Neurobiol. 2013;47:525–36.
9. Xu W, Tan L, Yu J-T. The link between the SNCA gene and parkinsonism. Neurobiol Aging. 2015;36:1505–18.
10. De Vos KJ, Mórotz GM, Stoica R, Tudor EL, Lau K-F, Ackerley S, et al. VAPB interacts with the mitochondrial protein PTPIP51 to regulate calcium homeostasis. Hum Mol Genet. 2011;21:1299–311.
11. Paillusson S, Gomez-Suaga P, Stoica R, Little D, Gissen P, Devine MJ, et al. α-Synuclein binds to the ER–mitochondria tethering protein VAPB to disrupt Ca2+ homeostasis and mitochondrial ATP production. Acta Neuropathol. 2017;134:129–49.
12. Wakabayashi K, Mori F, Nishie M, Oyama Y, Kurihara A, Yoshimoto M, et al. An autopsy case of early ("minimal change") olivopontocerebellar atrophy (multiple system atrophy-cerebellar). Acta Neuropathol. 2005;110:185–90.
13. Martín-Belmonte A, Aguado C, Alfaro-Ruíz R, Moreno-Martínez AE, de la Ossa L, Martínez-Hernández J, et al. Reduction in the neuronal surface of post and presynaptic GABAB receptors in the hippocampus in a mouse model of Alzheimer's disease. Brain Pathol. 2020;30:554–75.
14. Kamemura K, Chihara T. Multiple functions of the ER-resident VAP and its extracellular role in neural development and disease. J Biochem. 2019;165:391–400.
15. Mori F, Piao YS, Hayashi S, Fujiwara H, Hasegawa M, Yoshimoto M, et al. Alpha-synuclein accumulates in Purkinje cells in Lewy body disease but not in multiple system atrophy. J Neuropathol Exp Neurol. 2003;62:812–9.
16. Tanji K, Tanaka T, Mori F, Kito K, Takahashi H, Wakabayashi K, et al. NUB1 suppresses the formation of Lewy body-like inclusions by proteasomal degradation of synphilin-1. Am J Pathol. 2006;169:553–65.
17. Tanji K, Mori F, Kakita A, Zhang H, Kito K, Kamitani T, et al. Immunohistochemical localization of NUB1, a synphilin-1-binding protein, in neurodegenerative disorders. Acta Neuropathol. 2007;114:365–71.
18. Li J, Ma W, Li H, Hou N, Wang X, Kim IM, et al. NEDD8 ultimate buster 1 long (NUB1L) protein suppresses atypical neddylation and promotes the proteasomal degradation of misfolded proteins. J Biol Chem. 2015;290:23850–62.
19. Lau DHW, Paillusson S, Hartopp N, Rupawala H, Mórotz GM, Gomez-Suaga P, et al. Disruption of endoplasmic reticulum-mitochondria tethering proteins in post-mortem Alzheimer's disease brain. Neurobiol Dis. 2020;143:105020.
20. Bendor JT, Logan TP, Edwards RH. The function of alpha-synuclein. Neuron. 2013;79:1044–66.
21. Bartels T, Choi JG, Selkoe DJ. α-Synuclein occurs physiologically as a helically folded tetramer that resists aggregation. Nature. 2011;477:107–10.
22. Flagmeier P, Meisl G, Vendruscolo M, Knowles TP, Dobson CM, Buell AK, et al. Mutations associated with familial Parkinson's disease alter the initiation and amplification steps of alpha-synuclein aggregation. Proc Natl Acad Sci U S A. 2016;113:10328–33.
23. Miki Y, Tanji K, Mori F, Kakita A, Takahashi H, Wakabayashi K. PLA2G6 accumulates in Lewy bodies in PARK14 and idiopathic Parkinson's disease. Neurosci Lett. 2017;645:40–5.
24. Shahmoradian SH, Lewis AJ, Genoud C, Hench J, Moors TE, Navarro PP, et al. Lewy pathology in Parkinson's disease consists of crowded organelles and lipid membranes. Nat Neurosci. 2019;22:1099–109.
25. Mori A, Imai Y, Hattori N. Lipids: key players that modulate α-synuclein toxicity and neurodegeneration in Parkinson's disease. Int J Mol Sci. 2020;21:3301.
26. Papp MI, Kahn JE, Lantos PL. Glial cytoplasmic inclusions in the CNS of patients with multiple system atrophy (striatonigral degeneration, olivopontocerebellar atrophy and Shy-Drager syndrome). J Neurol Sci. 1989;94:79–100.
27. Kato S, Nakamura H. Cytoplasmic argyrophilic inclusions in neurons of pontine nuclei in patients with olivopontocerebellar atrophy: immunohistochemical and ultrastructural studies. Acta Neuropathol. 1990;79:584–94.
28. Duffy PE, Tennyson VM. Phase and electron microscopic observations of Lewy bodies and melanin granules in the substantia nigra and locus caeruleus in Parkinson's disease. J Neuropathol Exp Neurol. 1965;24:398–414.
29. Abe H, Yagishita S, Amano N, Iwabuchi K, Hasegawa K, Kowa K. Argyrophilic glial intracytoplasmic inclusions in multiple system atrophy: immunocytochemical and ultrastructural study. Acta Neuropathol. 1992;84:273–7.
30. Arima K, Murayama S, Mukoyama M, Inose T. Immunocytochemical and ultrastructural studies of neuronal and oligodendroglial cytoplasmic inclusions in multiple system atrophy. 1. Neuronal cytoplasmic inclusions. Acta Neuropathol. 1992;83:453–60.
31. Arima K, Ueda K, Sunohara N, Arakawa K, Hirai S, Nakamura M, et al. NACP/alpha-synuclein immunoreactivity in fibrillary components of neuronal and oligodendroglial cytoplasmic inclusions in the pontine nuclei in multiple system atrophy. Acta Neuropathol. 1998;96:439–44.
32. Chiba Y, Takei S, Kawamura N, Kawaguchi Y, Sasaki K, Hasegawa-Ishii S, et al. Immunohistochemical localization of aggresomal proteins in glial cytoplasmic inclusions in multiple system atrophy. Neuropathol Appl Neurobiol. 2012;38:559–71.
33. Gai WP, Power JH, Blumbergs PC, Culvenor JG, Jensen PH. Alpha-synuclein immunoisolation of glial inclusions from multiple system atrophy brain tissue reveals multiprotein components. J Neurochem. 1999;73:2093–100.
34. Kato S, Shinozawa T, Takikawa M, Kato M, Hirano A, Awaya A, et al. Midkine, a new neurotrophic factor, is present in glial cytoplasmic inclusions of multiple system atrophy brains. Acta Neuropathol. 2000;100:481–9.
35. Mochizuki A, Mizusawa H, Ohkoshi N, Yoshizawa K, Komatsuzaki Y, Inoue K, et al. Argentophilic intracytoplasmic inclusions in multiple system atrophy. J Neurol. 1992;239:311–6.
36. Murayama S, Arima K, Nakazato Y, Satoh J, Oda M, Inose T. Immunocytochemical and ultrastructural studies of neuronal and oligodendroglial cytoplasmic inclusions in multiple system atrophy. 2. Oligodendroglial cytoplasmic inclusions. Acta Neuropathol. 1992;84:32–8.
37. Nishie M, Mori F, Yoshimoto M, Takahashi H, Wakabayashi K. A quantitative investigation of neuronal cytoplasmic and intranuclear inclusions in the pontine and inferior olivary nuclei in multiple system atrophy. Neuropathol Appl Neurobiol. 2004;30:546–54.
38. Papp MI, Lantos PL. The distribution of oligodendroglial inclusions in multiple system atrophy and its relevance to clinical symptomatology. Brain. 1994;117(Pt 2):235–43.
39. Pountney DL, Dickson TC, Power JH, Vickers JC, West AJ, Gai WP. Association of metallothionein-III with oligodendroglial cytoplasmic inclusions in multiple system atrophy. Neurotox Res. 2011;19:115–22.

40. Shibuya K, Nagatomo H, Iwabuchi K, Inoue M, Yagishita S, Itoh Y. Asymmetrical temporal lobe atrophy with massive neuronal inclusions in multiple system atrophy. J Neurol Sci. 2000;179:50–8.
41. Shibuya K, Uchihara T, Nakamura A, Ishiyama M, Yamaoka K, Yagishita S, et al. Reversible conformational change of tau2 epitope on exposure to detergent in glial cytoplasmic inclusions of multiple system atrophy. Acta Neuropathol. 2003;105:508–14.
42. Takeda A, Arai N, Komori T, Kato S, Oda M. Neuronal inclusions in the dentate fascia in patients with multiple system atrophy. Neurosci Lett. 1997;227:157–60.
43. Tu PH, Galvin JE, Baba M, Giasson B, Tomita T, Leight S, et al. Glial cytoplasmic inclusions in white matter oligodendrocytes of multiple system atrophy brains contain insoluble alpha-synuclein. Ann Neurol. 1998;44:415–22.
44. Yokoyama T, Kusunoki JI, Hasegawa K, Sakai H, Yagishita S. Distribution and dynamic process of neuronal cytoplasmic inclusion (NCI) in MSA: correlation of the density of NCI and the degree of involvement of the pontine nuclei. Neuropathology. 2001;21:145–54.
45. Yu S, Li X, Liu G, Han J, Zhang C, Li Y, et al. Extensive nuclear localization of alpha-synuclein in normal rat brain neurons revealed by a novel monoclonal antibody. Neuroscience. 2007;145:539–55.
46. Monti B, Polazzi E, Batti L, Crochemore C, Virgili M, Contestabile A. Alpha-synuclein protects cerebellar granule neurons against 6-hydroxydopamine-induced death. J Neurochem. 2007;103:518–30.
47. Sangchot P, Sharma S, Chetsawang B, Porter J, Govitrapong P, Ebadi M. Deferoxamine attenuates iron-induced oxidative stress and prevents mitochondrial aggregation and alpha-synuclein translocation in SK-N-SH cells in culture. Dev Neurosci. 2002;24:143–53.
48. Xu S, Zhou M, Yu S, Cai Y, Zhang A, Ueda K, et al. Oxidative stress induces nuclear translocation of C-terminus of alpha-synuclein in dopaminergic cells. Biochem Biophys Res Commun. 2006;342:330–5.
49. Schneider BL, Seehus CR, Capowski EE, Aebischer P, Zhang S-C, Svendsen CN. Over-expression of alpha-synuclein in human neural progenitors leads to specific changes in fate and differentiation. Hum Mol Genet. 2007;16:651–66.
50. Cevc G, Richardsen H. Lipid vesicles and membrane fusion. Adv Drug Deliv Rev. 1999;38:207–32.
51. Matsumoto J, Stewart T, Sheng L, Li N, Bullock K, Song N, et al. Transmission of alpha-synuclein-containing erythrocyte-derived extracellular vesicles across the blood-brain barrier via adsorptive mediated transcytosis: another mechanism for initiation and progression of Parkinson's disease? Acta Neuropathol Commun. 2017;5:71.
52. Shi M, Liu C, Cook TJ, Bullock KM, Zhao Y, Ginghina C, et al. Plasma exosomal alpha-synuclein is likely CNS-derived and increased in Parkinson's disease. Acta Neuropathol. 2014;128:639–50.
53. Peng C, Trojanowski JQ, Lee VM. Protein transmission in neurodegenerative disease. Nat Rev Neurol. 2020;16:199–212.

How to cite this article: Mori F, Miki Y, Tanji K, Kon T, Tomiyama M, Kakita A, et al. Role of VAPB and vesicular profiles in α-synuclein aggregates in multiple system atrophy. *Brain Pathology*. 2021;31:e13001. https://doi.org/10.1111/bpa.13001